Mechanics & Industry **21**, 610 (2020)
© AFM, EDP Sciences 2020
https://doi.org/10.1051/meca/2020077

Mechanics & Industry

Available online at:
www.mechanics-industry.org

Regular Article

Mechanism of irregular crack-propagation in thermal controlled fracture of ceramics induced by microwave

Xiaoliang Cheng, Chunyang Zhao*, Hailong Wang, Yang Wang, and Zhenlong Wang

School of mechatronics engineering, Harbin Institute of Technology, Harbin 150001, PR China

Received: 18 March 2020 / Accepted: 28 September 2020

Abstract. Microwave cutting glass and ceramics based on thermal controlled fracture method has gained much attention recently for its advantages in lower energy-consumption and higher efficiency than conventional processing method. However, the irregular crack-propagation is problematic in this procedure, which hinders the industrial application of this advanced technology. In this study, the irregular crack-propagation is summarized as the unstable propagation in the initial stage, the deviated propagation in the middle stage, and the non-penetrating propagation in the end segment based on experimental work. Method for predicting the unstable propagation in the initial stage has been developed by combining analytical models with thermal-fracture simulation. Experimental results show good agreement with the prediction results, and the relative deviation between them can be <5% in cutting of some ceramics. The mechanism of deviated propagation and the non-penetrating propagation have been revealed by simulation and theoretical analysis. Since this study provides effective methods to predict unstable crack-propagation in the initial stage and understand the irregular propagation mechanism in the whole crack-propagation stage in microwave cutting ceramics, it is of great significance to the industrial application of thermal controlled fracture method for cutting ceramic materials using microwave.

Keywords: Crack-propagation / thermal controlled fracture method / microwave / ceramics / unstable propagation

1 Introduction

The application of advanced ceramic has become more and more widely and it is an indispensable material in high-tech intensive fields such as aerospace. Most of the occasions that ceramics are competent mainly relay on its unique properties such as high hardness, high melting point and low thermal expansion. However, these excellent properties make the cutting procedure difficult. In conventional cutting technic, material-removal process is almost ineluctable in both mechanical mode and thermal mode [1–3]. Generally, material-removal process would cause high energy-consumption, redundant material-waste and environmental pollution, and induce poor surface integrity and low processing precision [1–5]. Moreover, material-removal process by mechanical force would encounter serious tool wear as well as high processing cost.

Unlike these conventional cutting technic, thermal controlled fracture method (TCFM) is a green and pollution-free cutting mode, which uses tensile stress to separate the brittle material into two parts. The tensile stress is usually thermal stress induced by a heat source. Because this process only needs to overcome the surface energy between the new sections, it causes no material-removal. The TCFM was invented by Lumley et al in 1969, and was mainly used to treat glass sheets [6]. At the early stage, CO_2 laser with wavelength of 10.6 μm was used as heat source to induce thermal stress, which can only be absorbed on the surface of the glass and would not cutoff glass thoroughly. This always needs some subsequent breaking process. Then, some scholars found that laser with wavelength of 1064 nm could penetrate a certain thickness of glass to form a full-body cutting mode, and the priority of this cutting mode has been demonstrated [7–9].

During the development of half a century, scholars in this community have carried out many experimental and theoretical research on monocrystalline silicon, polycrystalline silicon, glass/silicon two-layer bonding materials and some ceramics [10–15]. The main difference between these materials and glass is that they can't form a full-body cutting mode with the commonly used laser wavelength. During laser cutting silicon sheets (usually <0.5 mm) process, it is generally considered that laser produces

* e-mail: zcytougao@163.com

a surface heat source with a negligible laser-absorption depth [12–15]. In other words, laser is absorbed at the surface of the silicon wafer, and the heat in the whole thickness is mainly generated by heat transfer.

In the past, TCFM is mainly used to treat these thin plates [16,17]. Although it has also been used to cut thick ceramics, the TCFM induced by laser is reported not competent for high-quality cutting process. This is because that laser is not easy to induce full-body cutting mode for ceramics [18,19]. Wang et al. first proposed to use microwave to treat ceramics based on TCFM [20]. They have successfully cut SiC ceramic with a thickness of 3 mm with full-body cutting mode. However, some ceramics are difficult to absorb microwave, even though they could be completely penetrated. Then, Wang et al. used graphite to coat the surface of these ceramics to realize TCFM based on micro-discharge mechanism. Although under the similar mode of surface absorption, the micro-discharge makes its cutting quality better than that of laser cutting [18,19,21].

Wang et al. have found that crack-propagation path always deviates from the expected propagation path during TCFM [20–22]. This irregular crack-propagation hinders the industrial application of this advanced process. To deal with this problem, it is important to understand the mechanism of irregular crack-propagation. However, there are few reports on this issue.

In this paper, analytical models have been developed to reveal the irregular crack-propagation mechanism in microwave cutting ceramics using TCFM. Simulation of thermal fracture was conducted by general finite element simulation software to simulate the temperature and stress distribution. Combining the analytical models with the simulation work, the prediction of the maximum deviation range and the initial unstable crack-propagation length have achieved. Microwave cutting experiments with regards to glass, SiC, Al_2O_3 and ZrO_2 ceramics were conducted to verify this prediction method. Simulation work was also used to reveal the mechanism of the irregular crack-propagation in the middle stage and end segment.

2 Materials and Method

2.1 Principle of microwave cutting ceramics based on thermal controlled fracture method

The main physical process in the microwave cutting ceramics based on TCFM is shown in Figure 1. It can be divided into three procedures. Firstly, microwave heating ceramics as shown in Figure 1a: this process mainly consists of the dielectric loss of ceramic materials to microwave, the generation and conduction of heat. The incident microwave could penetrate the ceramics and be absorbed by the materials. According to absorptive capacity to microwave, it can be divided into bulk- heating mode (ceramics can absorb microwave well by themselves) and surface heating mode (coating graphite on ceramics to add absorption of microwave); secondly, the generation of thermal stress as shown in Figure 1b: this process is mainly based on the theory of thermal stress. Tensile stress occurs where temperature is lower than the average value, while compressive stress occurs where temperature is above the average value. The absolute value of thermal stress is mainly determined by the temperature gradient. Finally, the crack propagation process as shown in Figure 1c: this process is mainly based on the theory of fracture mechanics of solid materials. When the initial crack on the ceramic encounters a tensile stress greater than the fracture strength of the ceramic, it will propagate. If the tensile stress can guide the crack to propagate continuously at a certain speed, the cutting process achieves.

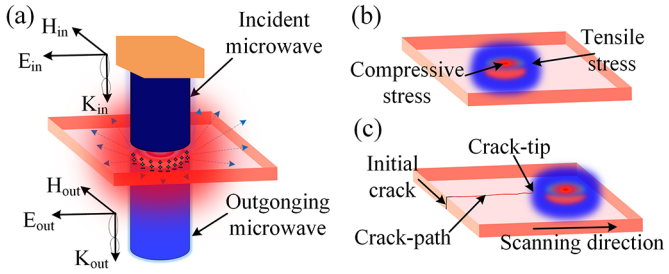

Fig. 1. Physical processes ((a) microwave heating ceramics, (b) generating thermal stress and (c) crack propagation process) in microwave cutting ceramics based on TCFM.

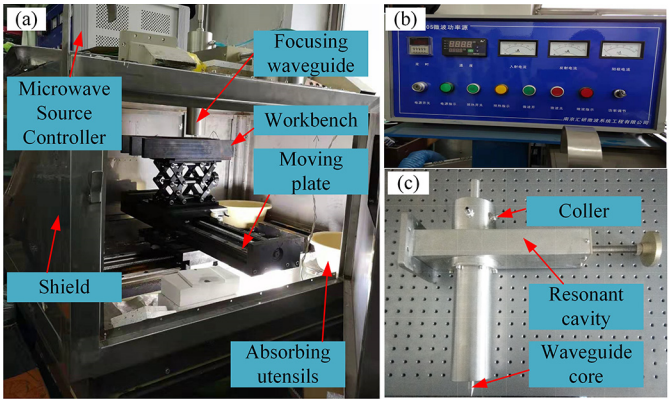

Fig. 2. Experimental apparatus of microwave cutting system consisting of (a) microwave source and cutting machine, (b) microwave controller and (c) circular focusing waveguide.

2.2 Experimental equipment, materials, and methods

Figure 2 shows the experimental apparatus of microwave cutting system. It is produced by Nanjing Huiyan Microwave System Engineering Co., Ltd of china and its maximum output power is 1.5 kW. The type used in this study is MY1500S. The system is composed of a microwave source and a cutting machine (2.45 GHz) shown in Figure 2a, microwave controller shown in Figure 2b, a x-y moving plate, and a circular focusing waveguide shown in Figure 2c. The circular focusing waveguide is used to generate circular heat source. Previous studies have shown that the circular heat source is more feasible for curve cutting of glass [22].

Table 1. Processing parameters in microwave cutting ceramic using TCFM.

Parameter	Glass plate	SiC plate	Al_2O_3 plate	ZrO_2 plate
Scanning velocity (mm/s)	0.4	0.2	0.6	1.5
Microwave power (kW)	1	1.5	0.5	0.5

To improve the security of the experiment, the inner wall of the machine tool shield is made of absorbing material, and four utensils containing water are placed into the cabin to absorb the leaky microwave during experiment. The material is placed on the workbench which could adjust the distance between the waveguide and workpiece.

The experimental materials include NaCa glass, SiC ceramic, Al_2O_3 ceramic and ZrO_2 ceramic. The dimensions of these materials are $100 \times 100 \times 1$ mm.

Curve cutting experiments are carried out. The start point of scanning position on the workpiece was marked in advance for recording the relative position of the crack-propagation path conveniently. Optical microscope was used to observe the crack-propagation path after the cutting experiments. The controllable processing parameters are microwave power and scanning speed. The values of these parameters for each material are given in Table 1. Each group of experimental parameters were tested six times repeatedly.

2.3 Simulation model for cutting ceramics based on thermal controlled fracture method

The main physical process during microwave cutting are microwave absorption, heat transfer, thermal induced stress and crack propagation. The modeling process are as following:

The thermal power density P_v in the workpiece when loading with microwave can be given by [23]:

$$P_v = 2\pi f \varepsilon_0 \varepsilon \tan\delta |E_{out}|^2 \tag{1}$$

where P_v is thermal power density (W/m^3); f is microwave frequency (Hz); ε_0 is vacuum dielectric constant (F/m); ε is relative dielectric constant of material; $tan\delta$ is dielectric loss tangent of material. $|E_{out}|$ is RMS of electric field intensity for output microwave (V/m).

When heated to a steady temperature, the temperature at any point in a linear elastic half space at the initial crack can be given by:

$$T(x,y,z) = \frac{P_v}{2\rho c a z'} \log\left(\frac{\sqrt{(x-x_0)^2+y^2}}{\sqrt{(x+x_0)^2+y^2}}\right) \tag{2}$$

where a is thermal conductivity (W/m$\cdot$°C), ρ is density (kg/m3), c is specific heat capacity (J/(kg$\cdot$°C), z' is workpiece thickness (m).

According to thermal stress theory, this would produce a thermal stress field in the material. The normal stress σ_x along X-direction and σ_y along Y-direction at any point at the initial crack caused by temperature field are given by:

$$\sigma_x = G\varepsilon_x - \beta T \tag{3}$$

and

$$\sigma_y = G\varepsilon_y - \beta T \tag{4}$$

where G is modulus of elasticity in shear, ε_x and ε_y are normal strain, β is thermal stress coefficient.

According to thermal stress theory of fracture mechanics of brittle solid materials, the critical fracture stress σ_F at the crack front can be given by [24]:

$$\sigma_F = [2E'\gamma/(\pi c_0)]^{1/2} \tag{5}$$

Where c_0 is the size of the pre-crack, γ is the free surface energy per unit area, E' is the equivalent modulus, which is equal to the elastic modulus E under the condition of thin specimen. When the thermal stress loaded at crack front is greater than or equal to σ_F, the crack system begins to expand.

The goal of analyzing the main physical process during microwave cutting is to simulate the dynamic process of crack-propagation. The crack-propagation process is discontinuous, so the conventional finite element method (FEM) can't be used to calculate the crack-propagation process directly. To resolve this problem, the extended finite element method (EFEM) is used. This method needn't to refine grid dynamically in simulation process, and it has good convergence characteristics when the mesh around the crack is subdivided to a certain extent. These simulations are implemented in commercial finite element software ABAQUS 6.14-1.

In the simulation model, the element type is C3D8R, and the material damage type is evolution damage. As shown in Figure 3, the grid density nearby the microwave scanning position is increased. In this way, the calculation results of the concerned areas become more accurate, and the calculation efficiency can be improved.

The physical parameters of the ceramics are shown in Table 2. The parameters are effective in room temperature, however, since the processing temperature of the TCFM is low (can be lower than 200 °C), these can also be used in the prediction model. Physical parameters given in the table include electromagnetic parameters, mechanical parameters and thermal parameters. The dielectric constants of these materials are provided by AET Corporation of Japan. The mechanical and thermal parameters of these materials are provided by Harbin Xinhui Special Ceramics Co., Ltd of china. According to the Equation (1), ε and tanδ are two material property which determines the microwave absorption and heat production capacity of materials.

Table 2. Physical parameters of the materials.

Physical parameters	Glass	SiC	Al_2O_3	ZrO_2	Graphite coating
Relative dielectric constant ε	6.8	12.226	7.3	3.2	15
Loss tangent $\tan\delta$	0.01	0.08	0.0003	0.0005	0.2
Thermal expansion coefficientα (10^{-6}/°C)	9	4	7.5	10.1	–
Modulus of elasticity E' (GPa)	68.9	360	370	200	–
Poisson's ratio v	0.23	0.142	0.22	0.25	–
Thermal conductivity a (W/m·°C)	3	40	25	7	–
Specific surface energy γ (N/m)	8	33.3	45	155	–
Density ρ (g/cm^3)	2.5	3.8	3.9	6.8	–
Specific heat c (J/Kg·°C)	835	450	880	450	–

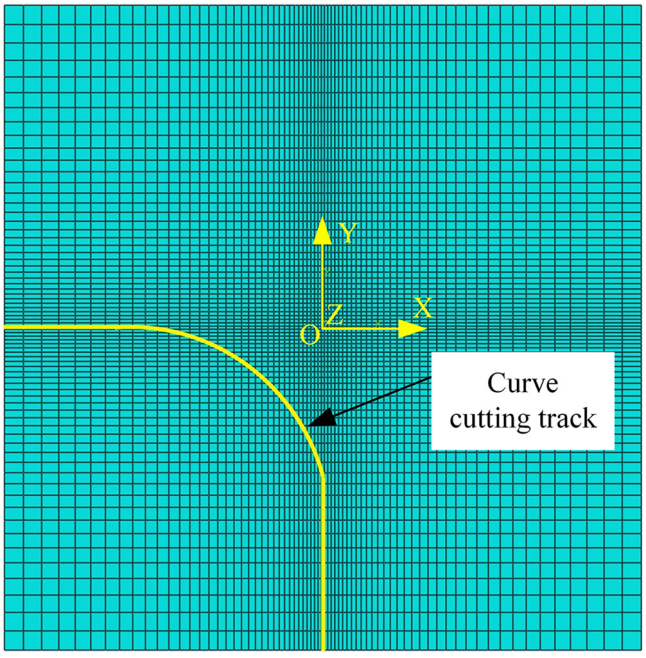

Fig. 3. Finite-element-meshes of cutting ceramics based on TCFM.

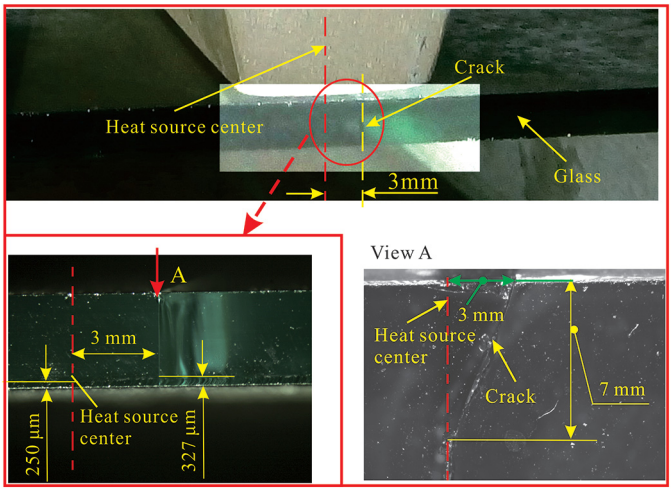

Fig. 4. Unstable propagation of initial crack of glass.

Among them, NaCa glass and SiC ceramic can absorb microwave of 2.45 GHz well. Al_2O_3 ceramic and ZrO_2 ceramic used in this study can hardly absorb microwave of this frequency band, so the surfaces of the radiation site are coated with graphite, which is good absorbing material for microwave. The ε and tanδ of the graphite coating are also given in the table, which are used in the cutting simulation of Al_2O_3 and ZrO_2.

3 Results

3.1 Crack-propagation in initial stage

To observe the crack-propagation state, cutting experiments on glass were conducted. Figure 4 shows the crack-propagation in the initial stage during cutting glass with microwave. When the initial crack propagates, it makes a sharp blasting noise. As shown in Figure 4, the initial crack-propagation deflects form the scanning path. The distance between the starting point of crack-propagation and the heat source center is defined as the starting point deviation (Y_1'). The length of the initial unstable propagation segment in scanning direction is defined as the unstable propagation length (X_1'). It is found that Y_1' is approximately 3 mm and X_1' is approximately 7 mm.

It is notable that micro-cracks on the left of the heat source center are about 250 μm, and micro-cracks on the right side are about 327 μm. As shown in Figure 4, the crack propagates from the micro-crack with 327 μm.

According to the Equation (5), the larger the crack size c_0, the smaller the critical stress σ_F is required for crack initiation. The critical stress corresponding to 327 μm is about 87.4% to it of 250 μm. The tensile stress at the crack front is determined by its distance from the heat source center. Therefore, for micro-cracks with same distance, these of 327 μm have greater opportunities to propagate than these of 250 μm.

3.2 Crack-propagation in middle and end stage

The crack-propagation morphology of curve cutting of glass is shown in Figure 5. The red reference line represents the scanning path. The crack-propagation path consists of

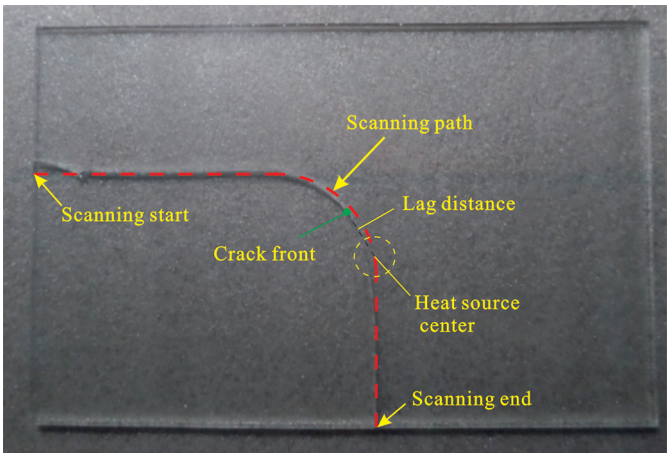

Fig. 5. Crack-propagation morphology of curve cutting of glass with circular microwave spot.

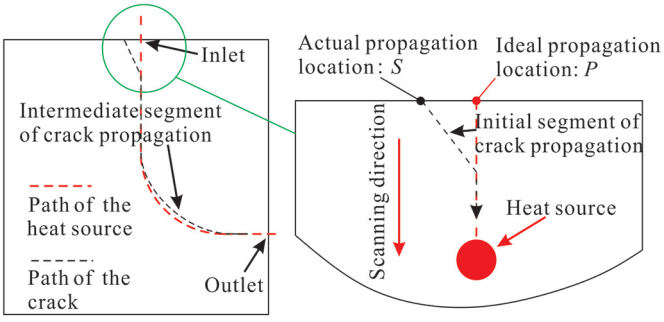

Fig. 6. Sketch of irregular crack-propagation in microwave cutting experiment.

an initial straight-line segment, a middle curve segment and a final straight-line segment. It is noteworthy that in the curve cutting segment the crack path deviates from the scanning path and inclines to the inside of the curve. There is a lag between the crack front and the heat source center in the curve cutting segment. The crack undergoes a non-penetrating propagation (the crack do not propagate close to the outlet of scanning) in the end segment.

4 Discussion

4.1 Prediction of the unstable crack-propagation in initial stage

The irregular crack-propagation phenomena shown in Figure 5 indicate that the realistic crack-propagation path is not along with the expected scanning path accurately. These non-ideal propagation phenomena can be simplified as a diagram shown in Figure 6. It shows that the actual crack initiation point S deflects from the ideal point P in the initial propagation stage. Because of this deflection, the initial realistic crack-propagation deflects from the ideal path (the microwave scanning path) evidently. In the intermediate segment, the crack path deviates from the heat source path obviously in curve cutting site. In the end segment, the crack does not penetrate the specimen in the outlet. In order to understand the mechanism of irregular crack-propagation, models for predicting the maximum crack initiation range and the length of the initial unstable crack-propagation have been established respectively.

In the fracture mode I, the critical conditions for crack initiation can be written as [24]:

$$K_I \geq K_{Ic} \tag{6}$$

where K_I is the stress intensity factors in fracture type I, K_{Ic} is the fracture toughness of an infinite plate with unilateral crack. According to theory of fracture mechanics, under the condition of edge crack, K_I can be written as:

$$K_I = 1.12\sigma_r\sqrt{\pi l_r} \tag{7}$$

where σ_r is tensile stress at the crack front without considering of stress concentration; l_r is the crack length. The K_{Ic} can be the expressed by:

$$K_{Ic} = 1.12\sigma_c\sqrt{\pi l_r} \tag{8}$$

where σ_c is the critical stress for crack initiation (when the tensile stress at crack front is beyond σ_c, the crack would propagate). It can also be written as:

$$K_{Ic} = 1.12\sigma_r\sqrt{\pi l_r} \tag{9}$$

where l_c is the critical crack-length for crack initiation. According to Equations (8) and (9), σ_c and l_c can be written by:

$$\sigma_c = \frac{K_{Ic}}{1.12\sqrt{\pi l_r}} \tag{10}$$

and

$$l_c = \frac{(K_{Ic})^2}{1.12^2\pi(\sigma_r)^2} \tag{11}$$

Equation (10) is the critical stress for crack-propagation and Equation (11) is the critical crack-length for crack-propagation. The crack initiation condition is: $\sigma_r \geq \sigma_c$ or $l_r \geq l_c$.

Generally, there are many micro-cracks on the edges of ceramic and glass workpieces as shown in Figure 4. Experimental results show that the crack system tends to trigger from the micro-cracks with longer length. These micro-cracks commonly distribute randomly with different length at the edge of workpiece. Reference to Figure 6, the ideal propagation location is P and the actually propagation location is S. According to Equation (10) and the crack initiation condition, the stress conditions for crack propagating from P not S are:

$$\begin{cases} \sigma_{rp} \geq \sigma_{cp} = \dfrac{K_{Ic}}{1.12\sqrt{\pi l_{rp}}} \\ \sigma_{rs} < \sigma_{cs} = \dfrac{K_{Ic}}{1.12\sqrt{\pi l_{rs}}} \end{cases} \tag{12}$$

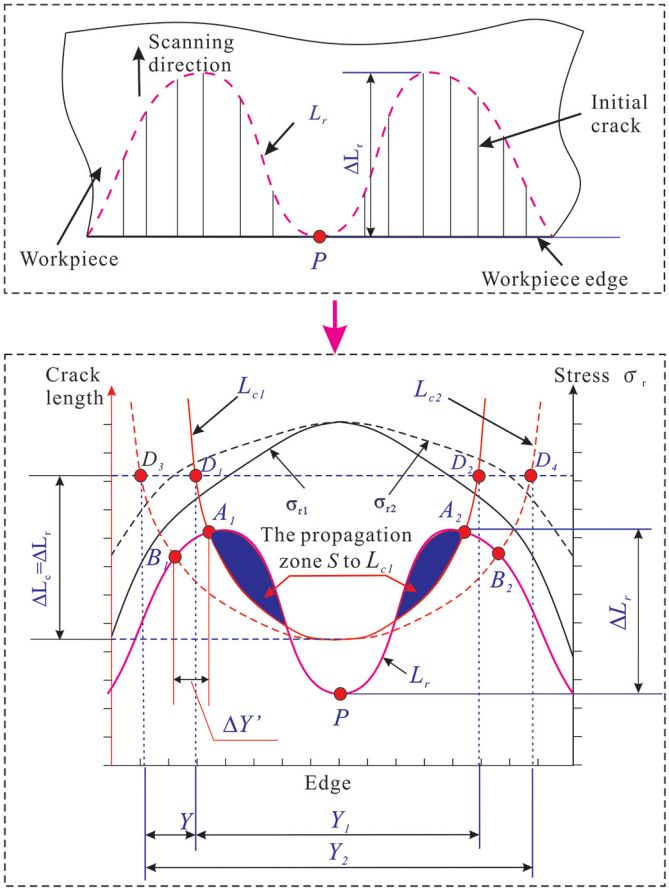

Fig. 7. Principle of determining the crack-propagation region under typical stress distribution conditions.

According to Equation (11) and the crack initiation condition, the crack-length conditions for crack propagating from P not S are:

$$\begin{cases} l_{rp} \geq l_{cp} = \dfrac{(K_{Ic})^2}{1.12^2\pi(\sigma_{rp})^2} \\ l_{rs} < l_{cs} = \dfrac{(K_{Ic})^2}{1.12^2\pi(\sigma_{rs})^2} \end{cases} \quad (13)$$

The meaning of these parameters consults the parameter description in Equations (9) and (10), just adding P or S as subscripts to represent the corresponding value in these two places shown in Figure 6.

Because of the random distribution of the micro-crack at the edge of specimen, the location of crack initiation is random and can't be accurately determined. However, the region of it could be predicted theoretically by analyzing the crack initiation condition above. Figure 7 shows the principle to predict the crack-propagation region under typical stress distribution conditions.

The curve L_r in Figure 7 represents the length variation of micro-crack along the edge of specimen. The crack length at the ideal position P is defined as the smallest one. The curves of σ_{r1} and σ_{r2} correspond to two different stress distribution curves. The curves of L_{c1} and L_{c2} represent the crack-length threshold curves corresponding to σ_{r1} and σ_{r2} respectively. The intersection of L_{c1} and L_r is A_1 and A_2; the intersection of L_{c2} and L_r is B_1 and B_2.

According to Equation (11), the closed shadow region of L_{c1} and L_r is the possible crack-propagation region under the condition of σ_{r1}. Because it satisfies the crack initiation condition of $l_r \geq l_c$ in this region. When the crack-length threshold curve is L_{c2}, the crack-propagation region would add a distance of $\Delta Y'$ that is the length between A_1 and B_1. However, it is difficult to predict A_1, A_2, B_1 and B_2 in practice.

To simplify the prediction process of crack-propagation region, D_1, D_2, D_3 and D_4 are introduced to replace the A_1, A_2, B_1 and B_2. The determination process and the meaning of these points are as followings:

1. The determination of D_1, D_2, D_3 and D_4:

First, obtaining the fluctuation value of crack-length as ΔL_r; then, drawing upwards a line whose distance from the bottom of curve L_{c1} and L_{c2} is ΔL_r; finally, the interactions between this line and the L_{c1} and L_{c2} are D_1, D_2, D_3 and D_4.

2. The meaning of D_1, D_2, D_3 and D_4:

D_1 and D_2 are the extreme location for crack initiation corresponding to σ_{r1}, and Y_1 is the maximum crack initiation range corresponding to σ_{r1}. Similarly, D_3 and D_4 are the extreme location for crack initiation to σ_{r2}, and Y_2 is the maximum crack initiation range corresponding to σ_{r2}.

3. Its relationship with A_1, A_2, B_1 and B_2:

When the lowest points of L_{c1} and L_{c2} are close to position P, D_1, D_2, D_3 and D_4 are approximately coincident with A_1, A_2, B_1 and B_2, and the ΔY (distance between D_1 and D_3) is approximately equal to $\Delta Y'$.

By introducing D_1, D_2, the step to obtain maximum crack initiation range Y_1 is as following:

Frist, σ_r curve is obtained by stress calculation or simulation; then, the corresponding curve Lc can be fitted using some discrete points calculated by Equation (9). Finally, the D_1, D_2 is obtained by the above methods, and the Y_1 is achieved.

By using this method, the maximum crack initiation ranges of the four kinds of specimens are gotten and are shown in Figure 8. The σ_r curve and L_c curve are obtained by thermal stress simulation. The length change of micro-crack in the edge of each workpiece is defined as $\Delta l_{\max}$ corresponding to Δl_{rc} in Figure 7. This value is obtained by calculating the length difference between the maximum value and the minimum value of the micro-cracks. Due to the different manufacturing methods of workpieces, these values for these four materials are different. After measurement and calculation, the $\Delta l_{\max}$ for glass is approximately 200 μm, as well as 500 μm for SiC, 400 μm for Al_2O_3 ceramic and 300 μm for ZrO_2 ceramic. As shown in Figure 8, it is found that the Y_1 for glass is approximately 6 mm as well as 12 mm for SiC, 8 mm for Al_2O_3 and 10 mm for ZrO_2.

Under the condition of a unilateral crack on a rectangular plate with unit thickness, if the crack length is x and an increment dx is added, according to the theory of Griffith energy release, then the released stress-strain

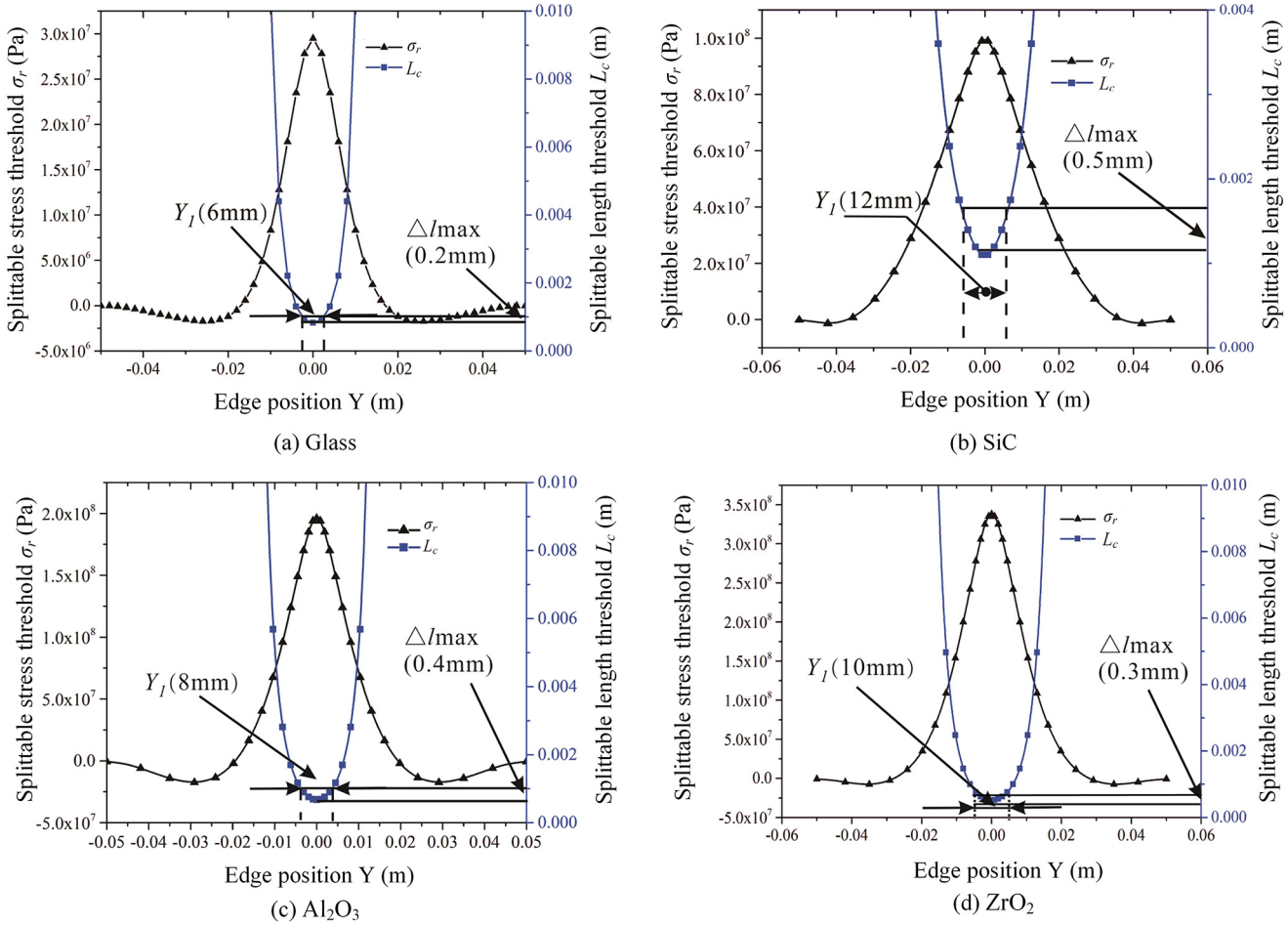

Fig. 8. Thermal stress and representative zone of crack along the cutting in edge of four kinds of ceramics.

energy dU_ε can be written as:

$$dU_\varepsilon = -\pi \frac{2(\sigma_f)^2}{E} x dx \tag{14}$$

where σ_f is the tensile stress perpendicular to the crack-front (Pa), which is balanced with the external load; The generated surface energy dE_s (J)is:

$$dE_\varepsilon = 2\gamma dx \tag{15}$$

When the crack propagates, the increment of kinetic energy is:

$$dE'_k = k\rho x v_s \frac{(\sigma_f)^2}{E} dx \tag{16}$$

Where k' is integral coefficient of displacement component; v_s is crack-propagation velocity (m/s); ρ is the reciprocal of acoustic velocity in the medium (s/m); E_k is crack kinetic energy (J).

The above energy meets the following requirements:

$$dU_\varepsilon + dE_s + dE_k = 0 \tag{17}$$

Introducing Equations (14)–(16) into Equation (17), then vs can be written as:

$$v_s \frac{\left(2\pi \frac{(\sigma_f)^2}{E} x - 2\gamma\right)}{k'\rho x \frac{(\sigma_f)^2}{E}} \tag{18}$$

When v_s is constant, the crack growth is stable. Then, σ_f can be written as:

$$\sigma_f = \frac{B_k}{\sqrt{x}} \tag{19}$$

where B_k is the constant of stress function, which can be written as:

$$B_k^2 = \frac{2\gamma E}{2\pi - k\rho v_s} \tag{20}$$

In actual thermal-cracking process, $k'\rho vs$ is negligible (because the crack-propagation is far less than acoustic

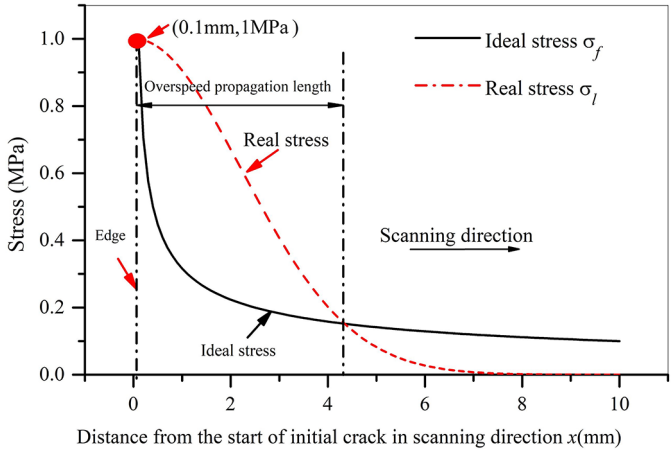

Fig. 9. Diagram of overspeed propagation length prediction.

velocity in the medium), so the stress σ_f can be written as:

$$\sigma_f = \sqrt{\frac{\gamma E}{\pi x}} \tag{21}$$

Equation (21) is an ideal stress condition in which the crack velocity is equal to the heat source velocity of a constant.

Due to the particularity of the boundary conditions of initial crack, the real stress σ_l in front of the crack is often greater than the ideal stress σ_f. This will induce the overspeed propagation of the initial crack. In theory, this unstable propagation segment tends to end when the stress-strain energy released by the crack system is equal to the surface energy produced by the newly generated surface.

Figure 9 shows the diagram of the relationship of these two stress curves and it can be used as a method to predict the overspeed propagation length. The distance between the specimen edge and the interaction of these two curves is the overspeed propagation length. It is apparent that the increase of the stress gradient in front of the crack tends to reduce the overspeed propagation length.

The prediction value of overspeed propagation length of each material is obtained and is shown in Figure 10. The intersection of σ_l curve and σ_f curve is defined as the stable point. The distance between the stable point and the workpiece edge is defined as overspeed propagation length X_1, which is actually the length of the initial unstable crack-propagation along X-direction (the microwave scanning direction).

Therefore, combining the σ_l curve and σ_f curve, the X_1 can be predicted. The σ_f curve can be obtained by Equation (21), while σ_l curve can be obtained by microwave cutting simulation. It indicates that X_1 of ZrO_2 ceramic is 10 mm; X_1 of Al_2O_3 ceramic is smallest, only 2 mm; X_1 of glass and SiC ceramic are 4.5 mm and 6 mm respectively.

Figure 11 shows the starting point deviation Y_1' and the unstable propagation length X_1' in cutting experiments of glass, SiC, Al_2O_3 and ZrO_2. The mean value and deviation value were calculated. Due to the different distribution of micro-cracks around workpiece edges and the unique mechanical and thermal properties of different materials, the mean values are different. As shown in Figure 11, it indicates that the results of Y_1' and X_1' fluctuates in cutting experiment of these materials.

Table 3 shows the comparation of experimental and predicted results on parameters in initial unstable propagation. It indicates that the mean values of Y_1' are not beyond half of the maximum crack initiation range Y_1. In the case of ZrO_2, $Y_1/2$ does not exceed 5% of the mean value of Y_1'. Combining with Figure 11, it is noteworthy that the maximum values of Y_1' do not deviate too much from half of Y_1. What' more, the mean value of X_1' does not deviate too much from the overspeed propagation length X_1. It indicates that the theoretical model can effectively predict the unstable propagation in the initial stage of microwave cutting ceramics based on TCFM.

4.2 Crack-propagation mechanism of middle and end stage

In the cutting experiments, the deviated crack-propagation appears in the middle stage of crack-propagation. In order to understand the mechanism of this phenomenon, the relationship between the tensile stress at the crack front and the propagation state of the crack was investigated. It is found that crack front does not always own the maximum tensile stress in the middle propagation segment. The crack front is sometimes at the front of the maximum tensile tress zone. This is the reason for discontinuous propagation of the intermediate crack. This is caused by the intermittent-equilibrium mechanism between the strain energy at the crack front and the newly generated surface energy for the newly propagated crack.

Figure 12 shows the relationship between the strain energy release and crack propagation at the crack front. The specific explanation is as follows: as shown in Figure 12a, tensile stress field is generated and concentrated around the crack front to balance with the compressive stress induced by the heat source center. This concentrated tensile stress would increase with the increase of its distance from the heat source. When the concentrated stress is greater than the threshold of the crack-propagation stress, the strain energy releases immediately and converts into surface energy for the generating new surface. At this moment, the new crack front can propagate instantaneously as shown in Figure 12b. Then, with the moving forward of heat source, the tensile stress at the crack front will gradually concentrate to its peak to induce a next propagation as shown in Figure 12c.

Therefore, to keep this cycle going, the maximum concentrated stress at the crack front should yield the tensile stress threshold for crack-propagation. If this maximum value can't reach the threshold in a segment, the tensile stress in the crack front would decrease as the heat source continues to go ahead. So, the crack-propagation would end. To avoid this phenomenon, the output power of microwave should not be less than a certain value.

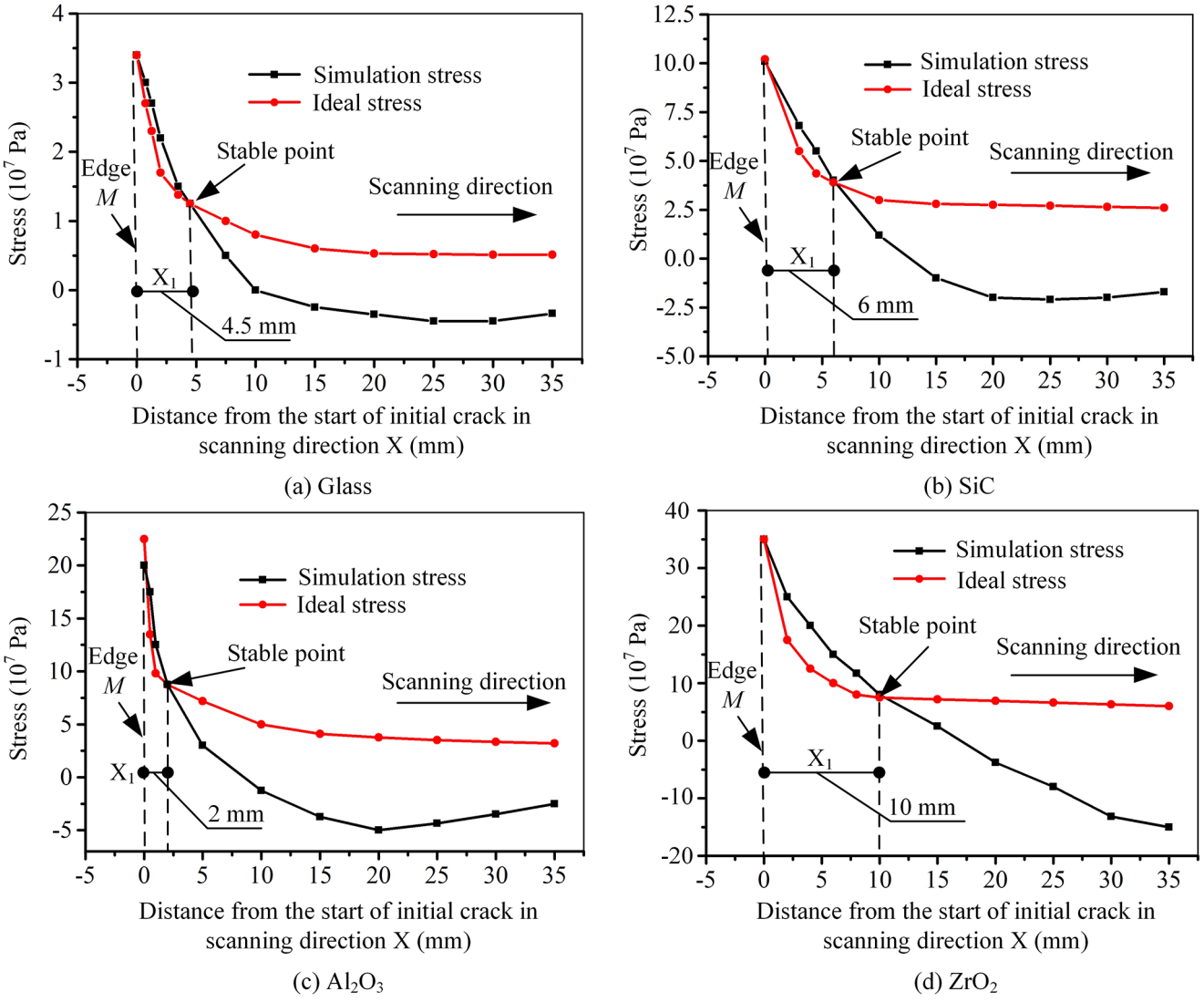

Fig. 10. Prediction results of overspeed propagation length of four kinds of ceramics.

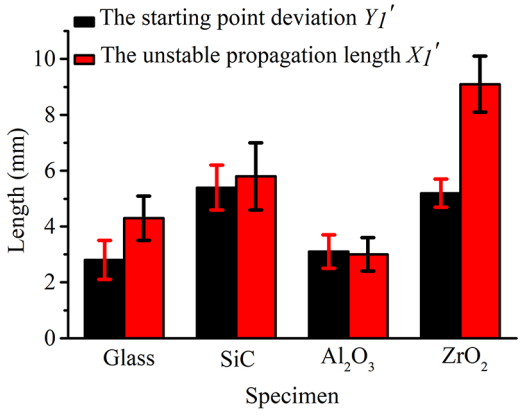

Fig. 11. Results of the starting point deviation length (Y_1') and the unstable propagation length (X_1') in the initial crack propagation stage.

Figure 13 shows a diagram of the relationship between the crack propagation path and the heat source path. When the heat source moves ahead, the crack will lag behind the heat source for a certain distance based on the intermittent propagation mechanism discussed above. As is shown in Figure 13, the crack always propagates towards the center of the heat source and keeps a distance of D_h from it. The actual propagation path of the crack is h_2 and is composed of a series of segments of broken line. When the broken line is short enough, its envelope curve (dotted line in the figure) is the actual crack-propagation path. It can be seen that the actual propagation path always deviates from the actual scanning trace in curve cutting.

Figure 14 shows one of the temperature field and tensile stress field contours in the process of curved-cracking of glass. As discussed above, the actual propagation path in curve cutting propagates into the inside of preset trace. This speculation reproduces in the simulation of curve cutting glass as shown in Figure 14. From the temperature

Table 3. Comparation of experimental and the prediction results on parameters in initial unstable propagation.

Materials	Experimental mean value of Y_1' (mm)	Prediction of Y_1 (mm)	Experimental mean value of X_1' (mm)	Prediction of X_1 (mm)
Glass	2.8	6	4.3	4.5
SiC	5.4	12	5.8	6
Al_2O_3	3.1	8	3.0	2
ZrO_2	5.2	10	9.1	10

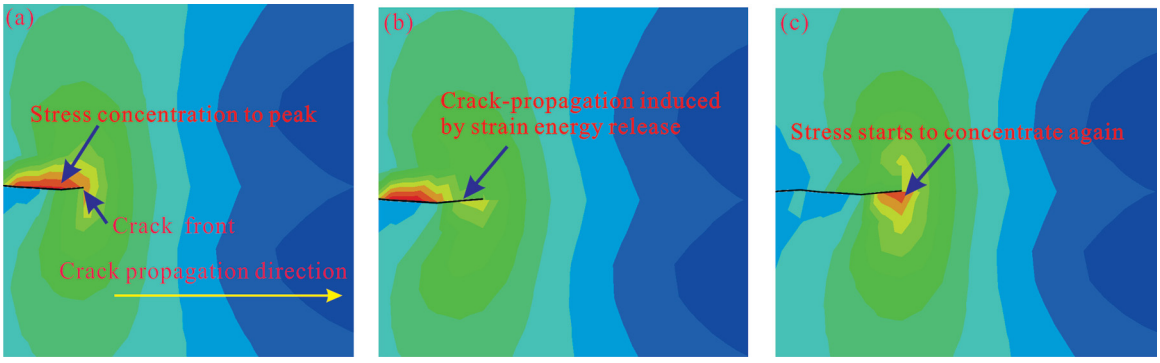

Fig. 12. Process of stain energy releasing and crack propagating. (a) Tensile stress field concentrating; (b) New crack front propagates; (c) A next propagation.

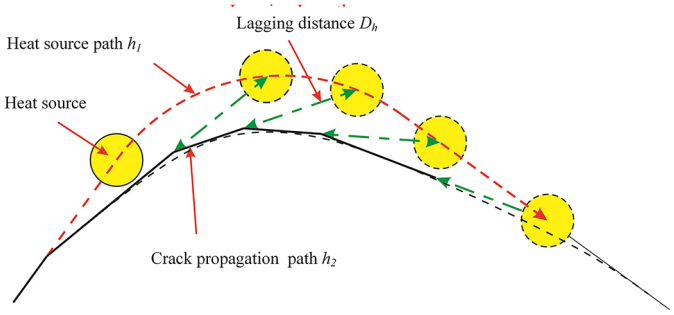

Fig. 13. Mechanism of deviation between cutting trajectory and heating path.

distribution contours in Figure 14a, it indicates that the maximum temperature in microwave cutting glass is about 140 °C, which is lower than the temperature value in laser cutting glass based on TCFM reported by Zhao [9]. Figure 14b shows simulation results of the stress distribution in curved-cracking of glass. As is shown in Figure 14b, the tensile stress is asymmetrically distributed along the scanning line.

According to the experimental results, the terminal crack failed to penetrate the workpiece. To reveal the reason for this phenomenon, the stress characteristic nearby crack front is analyzed when the crack propagates near the terminal point.

Figure 15 shows the simulation and sketch of the stress characteristic at the end propagation segment. As discussed above, the intermediate crack would undergo a discontinuous propagation caused by the intermittent-equilibrium mechanism between the strain energy at the crack front and the newly generated surface energy. However, this relative equilibrium state would be broken when the crack propagates near the end stage.

As shown in Figure 15a, a compressive stress field σ_{k1} is generated in the heating region. Tensile stress fields σ_{p1} and $\sigma p2$ would generate behind and in front of this compressive stress field to balance with it. In the middle segment, the tensile stress fields σ_{p1} and σ_{p2} are in equilibrium with the compressive stress field σ_{k1} as the heat source moving. However, this equilibrium no longer holds when the crack approaches the edge of the workpiece. As shown in Figure 15b, the distance between the center of $\sigma p2$ and workpiece edge is ΔD_k. When the heat source is close to the edge of the workpiece (ΔD_k is close to zero), the front tensile stress area σ_{p2} would produce a large stress concentration. Since the compressive stress in σ_{k1} is kept near constant, the average stress in σ_{p1} should decrease to keep balance. This decreases the stress intensity factor K at the crack front. When $K < K_{IC}$, the crack would stop propagating and result in non-penetrating propagation.

5 Conclusion

In conclusion, this paper has revealed the irregular propagation mechanism in the whole crack-propagation stage in microwave cutting ceramics using TCFM by experimental and theoretical study. The following conclusions can be drawn:

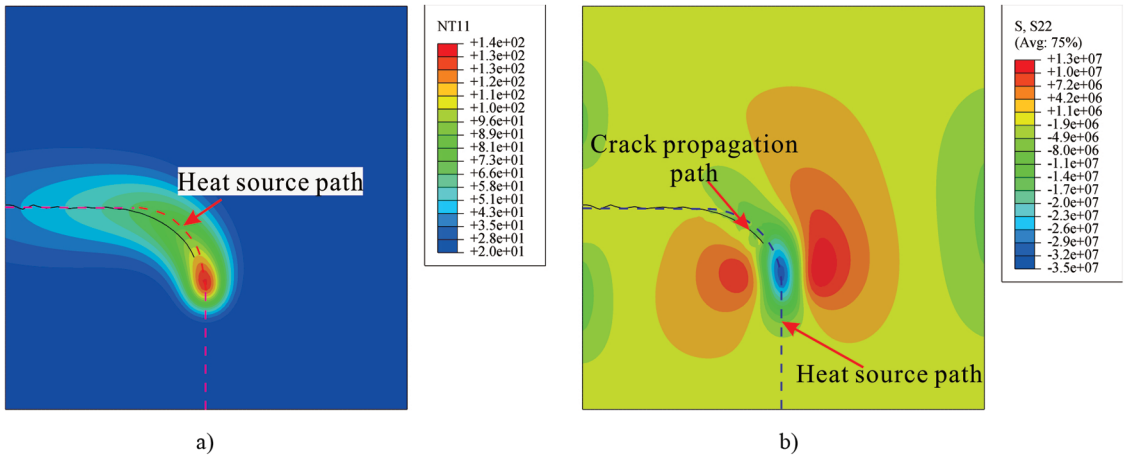

Fig. 14. Simulation of the deviated propagation in curved-cracking of glass and its corresponding temperature and stress distribution. (a) Temperature distribution (middle propagation). (b) Stress distribution (middle propagation).

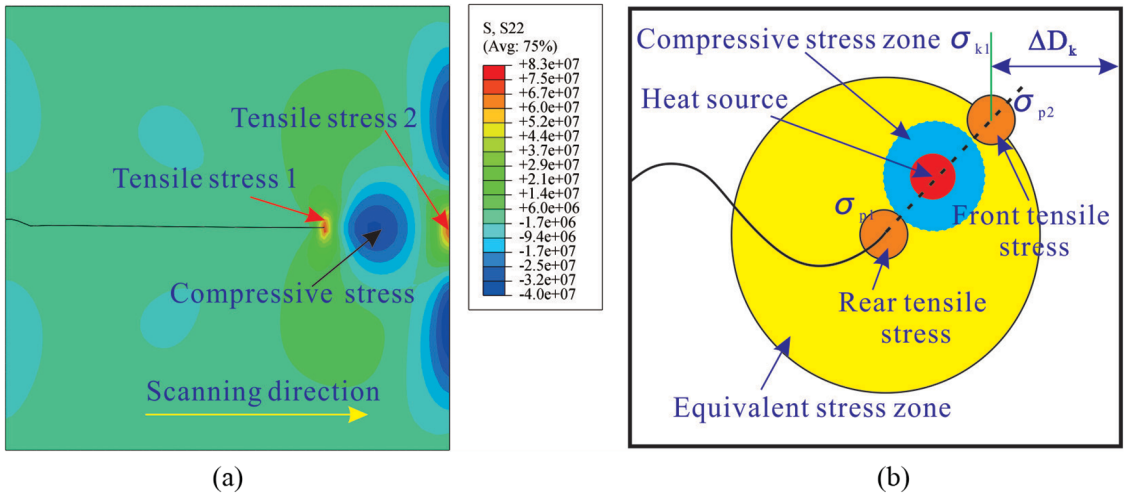

Fig. 15. Simulation and sketch of the stress state nearby the propagating crack at end segment. (a) Simulation of stress distribution. (b) Sketch of stress distribution.

– The phenomena of deviated crack propagation at the initial and intermediate segment and the non-penetrating propagation at the end segment were observed through curve cutting experiments. It indicates that the maximum temperature in microwave cutting glass is about 140 °C.
– The mechanism of the irregular crack-propagation was revealed by the combination of analytical model and finite element model. Through theoretical analysis, the propagation speed of the initial stage is higher than the scanning speed of microwave.
– The maximum crack initiation range and the length of the overspeed propagation could be predicted by analytical and finite element models. The microwave cutting experimental results show good agreement with the prediction results, and the relative deviation between them can be <5% in cutting of some ceramics.
– The crack front is sometimes in front of the maximum tensile tress. This is caused by the intermittent-equilibrium mechanism between the strain energy at the crack front and the newly generated surface energy.

By effectively predicting the unstable propagation offset and understanding the mechanism of irregular propagation, this study is of great significance to avoid and reduce the offset in thermal controlled fracture method using microwave.

This research is supported by the National Science Foundation of China (Grant No. 51275118).

References

[1] H. Aouici, M. Elbah, A. Benkhelladi, B. Fnides, L. Boulanouar, M.A. Yallese, Comparison on various machinability aspects between mixed and reinforced ceramics when machining hardened steels. Mechanics & Industry **20**, 109 (2019)
[2] S.N. Grigoriev, M.A. Volosova, S.V. Fedorov, E.A. Ostrikov, E.S. Mustafaev, K. Hamdy, The formation of the cutting tool microgeometry by pulsed laser ablation. Mechanics & Industry **19**, 703 (2018)

[3] B.S. Yilbas, S.S. Akhtar, C. Karatas. Laser cutting of alumina tiles: heating and stress analysis. J Manuf Process **15**, 14–24 (2013)
[4] M.A. Dabnun, M.S.J. Hashmi, M.A. El-Baradie, Surface roughness prediction model by design of experiments for turning machinable glass-ceramic (Macor). J. Mate. Process. Tech **164-165**, 1289–1293 (2005)
[5] Y. Luo, X. Wang, D. Wu, Quality investigation of alumina ceramic laser cutting based on vapor-to-melt ratio. J. Laser. Appl **30**, 032002 (2018)
[6] R.M. Lumley, Controlled separation of brittle materials using a laser, Am. Ceram. Soc. Bull **48**, 850–854 (1969)
[7] L.J. Yang, Y. Wang, Z.G. Tian, N. Cai, YAG laser cutting soda-lime glass with controlled fracture and volumetric heat absorption. Int. J. Mach. Tool. Manu **50**, 849–859 (2010)
[8] K.R. Kim, J.H. Kim, D.F. Farson, H.W. Choi, K.H. Kim, Hybrid laser cutting for flat panel display glass. Jpn. J. Appl. Phys **47**, 6978 (2008)
[9] C. Zhao, H. Zhang, L. Yang, Y. Wang, Y. Ding, Dual laser beam revising the separation path technology of laser induced thermal-crack propagation for asymmetric linear cutting glass. Int. J. Mach. Tool. Manu **106**, 43–55 (2016)
[10] O. Haupt, V. Schuetz, A. Schoonderbeek, L. Richter, R. Kling, High quality laser cleaving process for mono-and polycrystalline silicon. Proceedings of SPIE. 72020G-72020G-11 (2009)
[11] O. Haupt, F. Siegel, A. Schoonderbeek, Laser dicing of silicon: comparison of ablation mechanisms with a novel technology of thermally induced stress. J. Laser. Micro. Nanoen **3**, 135–140 (2008)
[12] A.M. Saman, T. Furumoto, T. Ueda, A. Hosokawa, A study on separating of a silicon wafer with moving laser beam by using thermal stress cleaving technique. J. Mate. Process. Tech **223**, 252–261 (2015)
[13] Y. Cai, L. Yang, H. Zhang, Y. Wang, Laser cutting silicon-glass double layer wafer with laser induced thermal-crack propagation. Opt. Laser. Eng **82**, 173–185 (2016)
[14] X. Cheng, L. Yang, M. Wang, Y. Cai, Y. Wang, Z. Ren, Laser beam induced thermal-crack propagation for asymmetric linear cutting of silicon wafer. Opt. Laser. Technol **120**, 105765 (2019)
[15] X. Cheng, L. Yang, M. Wang, Y. Cai, Y. Wang, Z. Ren, The unbiased propagation mechanism in laser cutting silicon wafer with laser induced thermal-crack propagation. Appl. Phys. A **125**, 479 (2019)
[16] T. Ueda, K. Yamada, K. Oiso, A. Hosokawa, Thermal stress cleaving of brittle materials by laser beam. CIRP Ann-Manuf. Technol **51**, 149–152 (2002)
[17] K. Yamada, T. Ueda, A. Hosokawa, Y. Yamane, K. Sekiya, Thermal damage of silicon wafer in thermal cleaving process with pulsed laser and CW laser. Proc of Spie, **6107**, 61070H–61070H-10 (2006)
[18] C.H. Tsai, C.J. Chen, Application of iterative path revision technique for laser cutting with controlled fracture. Opt. Laser. Eng **41**, 189–204 (2004)
[19] C.H. Tsai, H.W. Chen, Laser cutting of thick ceramic substrates by controlled fracture technique. J. Mate. Process. Tech **136**, 166–173 (2003)
[20] H. Wang, H. Zhang, Y. Wang, Splitting of glass and SiC ceramic sheets using controlled fracture technique with elliptic microwave spot. Ceram. Int. **43**, 1669–1676 (2016)
[21] H. Wang, H. Zhang, Y. Wang, M. Wang, Thermal controlled fracture of Al_2O_3 substrate by inducing microwave discharge in graphite coat. Ceram. Int **45**, 6149–6159 (2019)
[22] H. Wang, M. Wang, H. Zhang, Y. Wang, Use of inner-heated circular microwave spot to cut glass sheets based on thermal controlled fracture method. J. Mate. Process. Tech **276**, 116309 (2020)
[23] W.H. Sutton, Microwave processing of ceramic materials. Ceramic Bulletin **68**, 376–385 (1989)
[24] L. Brian, Fracture of brittle solids, second ed., Cambridge University Press. Cambridge University Press, 1993

Cite this article as: X. Cheng, C. Zhao, H. Wang, Y. Wang, Z. Wang, Mechanism of irregular crack-propagation in thermal controlled fracture of ceramics induced by microwave, Mechanics & Industry **21**, 610 (2020)